

ROLE OF BOND IN RC BEAMS STRENGTHENED WITH STEEL AND FRP PLATES

By Alessandra Aprile,¹ Member, ASCE, Enrico Spacone,² Associate Member, ASCE, and Suchart Limkatanyu³

ABSTRACT: This paper discusses the problem of predicting the stiffness, load capacity, and failure modes of RC members strengthened in bending with bonded steel or carbon-fiber-reinforced plastic thin plates. A critical issue of this strengthening technique is that, when the plate debonds, the load capacity suddenly drops and the failure mode is typically brittle. Because of the concrete cracking diffusion and the yielding of the steel rebars, a significant amplification of the bond stresses takes place at the beam-plate interface. Delamination occurs when the bond strength is reached locally. To properly describe and realistically predict the behavior of the strengthened beams, a displacement-based fiber beam model is used. Bond slip between the beam and the plate is included by assuming separate displacement fields in the beam and in the strengthening plate. The proposed model is used to confirm and investigate distinct failure modes observed in experimental investigations. The discussion is limited to shallow beams, where shear deformations are neglected.

INTRODUCTION

The rehabilitation and strengthening of insufficiently strong or damaged RC structures by means of externally bonded fiber-reinforced plastic (FRP) sheets has received great attention in recent years because of the diffusion of FRP materials in civil constructions and the parallel aging of the civil infrastructure in Europe, the United States, and Japan. This strengthening technique presents several practical advantages due to an easy installation on site, great geometrical flexibility, high strength-to-weight ratio, good durability, fatigue resistance, and low creep (Hollaway and Leeming 1999).

From the early 1990s, extensive experimental investigations on the structural behavior of FRP-strengthened RC beams have shown the significant improvement that can be obtained in structural performance, under both service and ultimate conditions. At the same time, the investigations have highlighted new brittle failure modes of the strengthened beams, mainly due to premature plate debonding [among others, Oehlers and Moran (1990), Saadatmanesh and Ehsani (1991), Arduini et al. (1997), Arduini and Nanni (1997), Hörmann (1997), and Zarnic et al. (1999)]. To predict the beam loading capacity and the failure mode due to plate debonding, it is important to use a model that can properly describe the bond stresses that develop at the strengthening plate-to-beam interface.

Several analytical and numerical solutions have been proposed in the published literature for the computation of the stresses that develop at the plate-to-beam interface in an uncracked RC beam (Roberts 1989; Täljsten 1997; Malek et al. 1998; Rabinovitch and Frostig 2000). In general, there are stresses acting both parallel to the interface (shear stresses) and normal to the interface (peeling stresses). All the elastic solutions in the references mentioned above stem from the assumption that the bending moment is carried partly by the RC beam in flexure and partly by the combined action of the strengthening plate in tension. The bending stiffness of the

strengthening plate is negligible when compared to the beam stiffness. Thanks to this assumption the interfacial shear stresses are easily computed by equilibrium and compatibility. Once the shear stresses are known, the peeling stresses are computed by following the elastic foundation analogy, where the adhesive layer is modeled as continuously distributed shear and vertical springs. Rabinovitch and Frostig (2000) presented a closed-form analytical model of the problem and showed that the obtained higher-order solution can be reduced to the simplified theories discussed above by omitting the appropriate terms. The available solutions indicate a distribution of shear and normal stresses along the plate length with the following characteristics:

- The shear stress is zero at the plate end and, over a very short length of plate of the order of the adhesive thickness, reaches its maximum value before decreasing.
- The peeling stress is significant over the same short length at the plate end and almost vanishes at a distance of about 3–4 times the adhesive thickness.

The maximum values of both shear and peeling stresses increase with the plate axial stiffness and with the distance of the plate free end from the beam supports. Although the available solutions shed light on the bonding problem, they have a limited effectiveness for the problem under study because they assume linear elastic material behavior and cannot consider concrete cracking diffusion or steel yielding at increasing load levels.

The available experimental evidence shows that plate debonding often occurs in intermediate areas, away from the plate end, where the concrete is cracked. Shear stress concentrations around flexural cracks and yielded steel areas may also lead to local debonding of the plate with a typical interface failure. On the other hand, when debonding starts from the plate end, where the concrete is uncracked, the local failure implies the detachment of the concrete cover with a typical shear failure. In this case, the failure is driven by a biaxial principal tension status composed by the interfacial stresses and the normal tension induced on concrete by the flexure (Saadatmanesh and Malek 1998). Based on the theory proposed by Täljsten (1997), the variation of the peeling stress/principal concrete stress ratio at the plate end with respect to the plate thickness is computed for the beams presented by Zarnic et al. (1999) and the results are plotted in Fig. 1. For cases of current practice where the strengthening plate is sufficiently thin, it can be easily verified that the influence of the

¹Asst. Prof., Dept. of Engrg., Univ. of Ferrara, Via Saragat 1, 44100 Ferrara, Italy.

²Assoc. Prof., Dept. of Civ., Envir., and Arch. Engrg., Univ. of Colorado, Boulder, CO 80309-0428.

³Doctoral Student, Dept. of Civ., Envir., and Arch. Engrg., Univ. of Colorado, Boulder, CO 80309-0428.

Note. Associate Editor: Joseph Bracci. Discussion open until May 1, 2002. To extend the closing date one month, a written request must be filed with the ASCE Manager of Journals. The manuscript for this paper was submitted for review and possible publication on January 23, 2001; revised May 24, 2001. This paper is part of the *Journal of Structural Engineering*, Vol. 127, No. 12, December, 2001. ©ASCE, ISSN 0733-9445/01/0012-1445-1452/\$8.00 + \$.50 per page. Paper No. 22694.

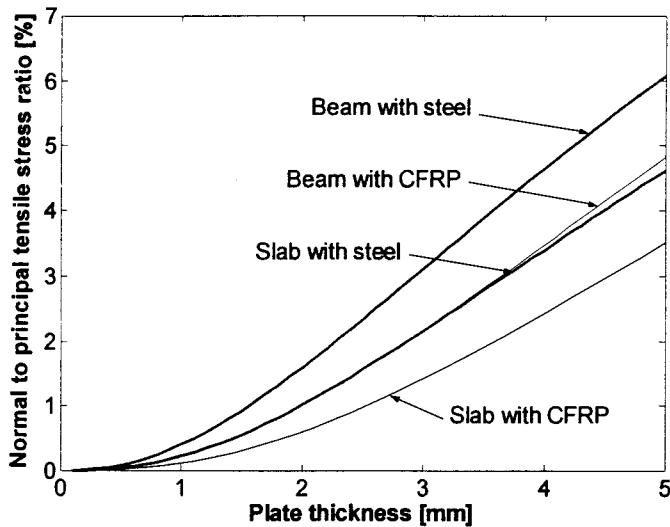


FIG. 1. Influence of Peeling Stress on Tensile Principal Stress

peeling stresses on the principal stresses is <5% and can thus be neglected for all practical purposes.

Based on the above considerations, the bond problem in RC beams strengthened with thin steel and FRP plates can be treated by neglecting the bending and shear stiffness of the strengthening plate. This greatly simplifies the bond problem and makes it quite similar to that of the steel rebars embedded in concrete. Design codes and frame finite elements with bond slip typically neglect stresses normal to the rebar axis. The study of bond slip is an important topic in RC modeling, under both static and dynamic excitations, because bond slip decreases the member stiffness and bond failure leads to premature, brittle member failure.

Significant advances in modeling the response of RC members were achieved in recent years, led by the development of beam models that rely on the fiber section model. Fiber section models naturally account for the coupling between axial and bending effects (Spacone et al. 1996) and can be combined with any beam element model, including displacement-based and force-based models. Fiber section models are typically based on the assumption that plane sections remain plane and thus neglect bond-slip effects. The bond-slip effects can be added in different ways: (1) by using nonlinear springs at the element ends (Rubiano-Benavides 1998) (this approach, however, is not readily extended to the study of RC beams strengthened with externally bonded thin plates); (2) by modifying the fiber section model to relax the compatibility between concrete and steel strains (Monti and Spacone 2000); and (3) by modeling the steel rebars and the concrete element with different degrees of freedom (Spacone and Limkatanyu 2000).

The numerical model used in this paper is based on the displacement-based RC frame element with bond slip proposed by Spacone and Limkatanyu (2000). The element is very easy to formulate and to implement. The model can properly describe the interfacial shear stress distributions that arise during loading of the RC beam up to failure. The peeling stresses normal to the rebars and to the plates are neglected. This model introduces an elastic-brittle bond law for the plate-concrete interface behavior and takes into account the nonlinear behavior of the materials including the tension stiffening of concrete in tensile areas. In the following, the RC frame element with bond slip is briefly reviewed, followed by an in-depth study of the response of RC beams strengthened by externally bonded steel and FRP plates. Available experimental data are used to validate the proposed modeling technique and to investigate different failure mechanisms.

DISPLACEMENT-BASED FIBER MODEL WITH BOND SLIP AND DEBONDING

The two-node displacement-based RC beam model used in this study is presented in Spacone and Limkatanyu (2000) and is shown in Fig. 2. The element formulation is briefly summarized hereafter. The original formulation considers slip in the steel rebars and in the bonded plate. In this study, slip is considered only between the concrete beam and the strengthening plate externally bonded at the beam top (in negative bending moment regions) or bottom (in positive moment regions). Plates bonded to the sides of the beams for shear strengthening are not considered, because this study focuses primarily on the flexural beam strengthening. The strengthening plates are assumed thin; thus, they only carry axial load and have no shear or flexural stiffness.

The RC beam element has two components: a two-node concrete beam and a strengthening plate. The nodal degrees of freedoms of the concrete beam and of the plate are different to permit slip. Fig. 2 shows the nodal displacements and the displacement fields along the element. The RC section is discretized into fibers. The element nodal displacements \mathbf{U} and the section displacements $\mathbf{u}(x)$ are also indicated in Fig. 2.

The section deformations are grouped in the vector $\mathbf{d}(x) = \{\epsilon_B(x) \ \kappa_B(x) \ | \ \bar{\epsilon}(x)\}^T$, where $\epsilon_B(x)$ is the beam axial strain, $\kappa_B(x)$ is the beam curvature, and $\bar{\epsilon}(x)$ is the plate axial strain. The RC beam formulation is based on the Euler-Bernoulli beam theory; thus, plane sections are assumed to remain plane. The RC section deformations are related to the beam displacements u_B and v_B through the compatibility relations $\epsilon_B = du_B/dx$ and $\kappa_B = dv_B/dx^2$. The plate axial strain $\bar{\epsilon}$ is the first derivative of the plate axial displacement \bar{u} ; i.e., $\bar{\epsilon} = d\bar{u}/dx$. The sections forces conjugate of $\mathbf{d}(x)$ are $\mathbf{D}(x) = \{N_B(x) \ M_B(x) \ | \ \bar{N}(x)\}^T$, where $N_B(x)$ and $M_B(x)$ are the RC section axial load and bending moment, respectively, and $\bar{N}(x)$ is the axial load in the strengthening plate. Finally, the slip $u_p(x)$ between the RC beam and the strengthening plate is $u_p(x) = \bar{u}(x) - u_B(x) + [dv_B(x)/dx]\bar{y}$, where $dv_B(x)/dx$ is the beam section rotation and \bar{y} is the plate distance from the beam reference axis, as indicated in Fig. 2.

The element displacements $\mathbf{u}(x)$ are expressed as functions of the nodal displacements \mathbf{U} through the shape functions $\mathbf{N}_u(x)$

$$\mathbf{u}(x) = \begin{Bmatrix} \mathbf{u}_B(x) \\ \bar{u}(x) \end{Bmatrix} = \begin{Bmatrix} \mathbf{N}_{uB}(x) \\ \mathbf{N}_u(x) \end{Bmatrix} \mathbf{U} = \mathbf{N}_u(x)\mathbf{U} \quad (1)$$

where $\mathbf{N}_{uB}(x)$ = array containing the shape functions of a two-node beam element. They are well-established functions that define a linear axial displacement field and a cubic vertical displacement field. The expression $\mathbf{N}_u(x)$ contains the shape functions of the plate with bond slip, which are linear in the present two-node formulation.

Beam and bond compatibility are both enforced in the strong form. The section and bond deformations are directly

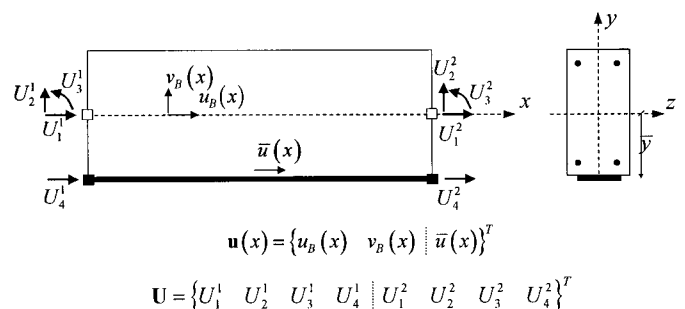


FIG. 2. Node and Element Displacements for RC Beam Model with Slip in Plate

related to the nodal displacements \mathbf{U} through the following equations:

$$\mathbf{d}(x) = \mathbf{B}_u(x)\mathbf{U}; \quad u_b(x) = \mathbf{B}_b(x)\mathbf{U} \quad (2)$$

where $\mathbf{B}_u(x) = \partial \mathbf{N}_u(x)$; $\mathbf{B}_b(x) = \partial_b \mathbf{N}_u(x)$; and ∂ and ∂_b = differential operators defined in the Notations.

Element equilibrium is enforced in the weak form. Application of the principle of virtual displacements, substitution of (2), and subsequent elimination of the virtual nodal displacements $\delta \mathbf{U}$ yield the following equilibrium statement:

$$\int_L \mathbf{B}_u^T(x) \mathbf{D}(x) dx + \int_L \mathbf{B}_b^T(x) D_b(x) dx = \mathbf{P} \quad (3)$$

where \mathbf{P} = nodal force vector conjugate of \mathbf{U} ; and $D_b(x)$ = bond force along the plate-to-beam interface. If (3) is rewritten in incremental form, the matrix form of element equilibrium becomes

$$\mathbf{K} \Delta \mathbf{U} = \mathbf{P} - \mathbf{P}^0 \quad (4)$$

where \mathbf{K} = element stiffness matrix, computed

$$\mathbf{K} = \mathbf{K}_B + \mathbf{K}_b \quad (5)$$

where \mathbf{K}_B and \mathbf{K}_b = beam and bond contributions to the element stiffness, respectively

$$\mathbf{K}_B = \int_L \mathbf{B}_u^T(x) \mathbf{k}_B(x) \mathbf{B}_u(x) dx; \quad \mathbf{K}_b = \int_L \mathbf{B}_b^T(x) k_b(x) \mathbf{B}_b(x) dx \quad (6)$$

where $\mathbf{k}_B(x)$ = RC beam section stiffness; and $k_b(x)$ = bond stiffness. \mathbf{P} is the array containing the element forces

$$\mathbf{P} = \mathbf{P}_B + \mathbf{P}_b \quad (7)$$

and $\mathbf{P}^0 = \mathbf{P}_B^0 + \mathbf{P}_b^0$ = array containing the element initial forces; \mathbf{P}_B = RC beam contribution to the element forces; and \mathbf{P}_b = contribution of the element with bond slip

$$\mathbf{P}_B = \int_L \mathbf{B}_u^T(x) \mathbf{D}_B(x) dx; \quad \mathbf{P}_b = \int_L \mathbf{B}_b^T(x) D_b(x) dx \quad (8)$$

In the present work, the fiber section model is used to compute the response of the RC beam section. Well-established uniaxial cyclic constitutive laws for the concrete, steel, and bond complete the element formulation. The loading envelopes of these laws are schematically shown in Fig. 3. The Kent and Park law (1971) is used for the concrete, with the addition of the tension response, which is assumed linear elastic up to the cracking stress f'_t , with rapid linear stress degradation for increasing tensile strains. The Menegotto and Pinto law (1973) is used for the steel rebars. For the bond between the concrete and the strengthening plate, a curve linear up to the point of bond failure is used. The above element formulation can be implemented in any general-purpose non-linear finite-element code. In the present study, the element is implemented in the program FEAP, documented in Taylor (1999).

COMPARISON OF EXPERIMENTAL AND ANALYTICAL STUDIES

The reference beams studied in this work are those tested at the University of Ljubljana, Slovenia, by Prof. R. Zarnic and coworkers and described in Zarnic et al. (1999). In the experimental program, 14 RC beams with different cross sections and strengthening materials were built and loaded to failure. Four-point bending tests were performed making use of a displacement controlled hydraulic actuator. Midspan displacements were measured by means of a couple of LVDTs, and

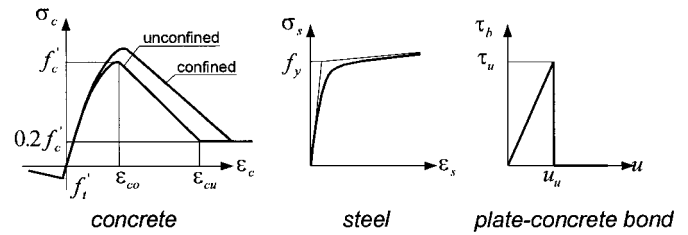


FIG. 3. Uniaxial Material Models

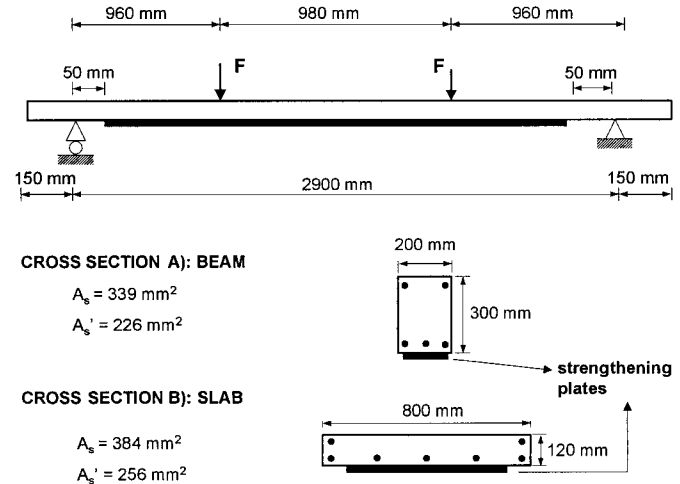


FIG. 4. Specimen Geometry and Test Layout for Beams Tested by Zarnic et al. (1999)

TABLE 1. Summary of Material Properties used by Zarnic et al. (1999)

Parameter	Elastic modulus (GPa)	Poisson's ratio ν	Compressive strength (MPa)	Tensile strength (MPa)
Concrete	27	0.2	25	3.5
Steel bars	210	0.3	460	460
Steel plate	210	0.3	360	360
CFRP plate	150	0.33	—	2,400
Epoxy resin	12.8	0.35	100	4 ^a

^aAdhesion for concrete surface.

strains on tensile concrete and plate surfaces were measured by placing strain gauges at the beam midspan and at the plate ends. As shown in Fig. 4, two different specimen types were cast for the tests: seven one-way slabs with an 800×120 mm² cross section and seven beams with a 200×300 mm² cross section. All the specimens had the same 3,200-mm length. The reinforcement steel ratio was set to 0.40% for the slabs and 0.56% for the beams, and 6-mm-diameter steel stirrups were placed at 100-mm intervals. Three beams for each group of specimens were externally strengthened with steel plates and three beams were strengthened with carbon FRP (CFRP) plates. A single, as-built beam for each group was used as the control specimen. The reinforcement plates were 50 and 100 mm wide for the beams and slabs, respectively. The steel and CFRP plates were 4 and 1.2 mm thick, respectively. For the plate bonding, the concrete surface was preventively polished and an approximately 2-mm-thick layer of epoxy resin was applied. A simple representation of the specimens' geometries and of the test layout are shown in Fig. 4, and the material mechanical properties were summarized in Table 1.

On the basis of the geometrical and mechanical data provided by Zarnic et al. (1999), a series of numerical tests were performed, making use of the frame model with bond slip

previously discussed. Thanks to the symmetry of the test setup, only half the specimen was considered for the numerical study. A mesh containing a total of 58 elements was used to obtain a sufficiently smooth response in terms of bond-stress distribution, although the overall applied load–midspan deflection response converged with as few as 15 elements. The nonlinear analyses were performed using a displacement-controlled technique based on a Newton-Raphson procedure (Bathe 1996).

For the bond model, a linear elastic bond law up to failure was considered for the interface between the concrete and the reinforcing plate (Fig. 3). This assumption is based on the actual elastic properties of the epoxy resin used for the connection, whereas the failure condition is mainly dependent on the concrete strength and surface preparation. Chajes et al. (1996) presented a detailed study on the bond strength of concrete-FRP glued joints subjected to shear stresses. The reported experimental data show that for this type of bond the shear strength typically ranges between 2 and 5 MPa, depending on the concrete surface layer quality. According to the mechanical properties of the epoxy resin used in the experimental tests by Zarnic et al. (1999), a bond elastic stiffness of 2,384 MPa/mm was assumed for the numerical investigations and a sound value of the bond strength was identified by comparing the numerical and the experimental results. Finally, the case with bond slip in the steel rebars was also considered, but it did not affect the results and did not yield additional information to the analyses. Rebar slip is therefore neglected in the following discussion.

In Fig. 5, the experimental and numerical results for the specimens by Zarnic et al. (1999) are compared in terms of applied load–midspan deflection for both the beams [Fig. 5(a)]

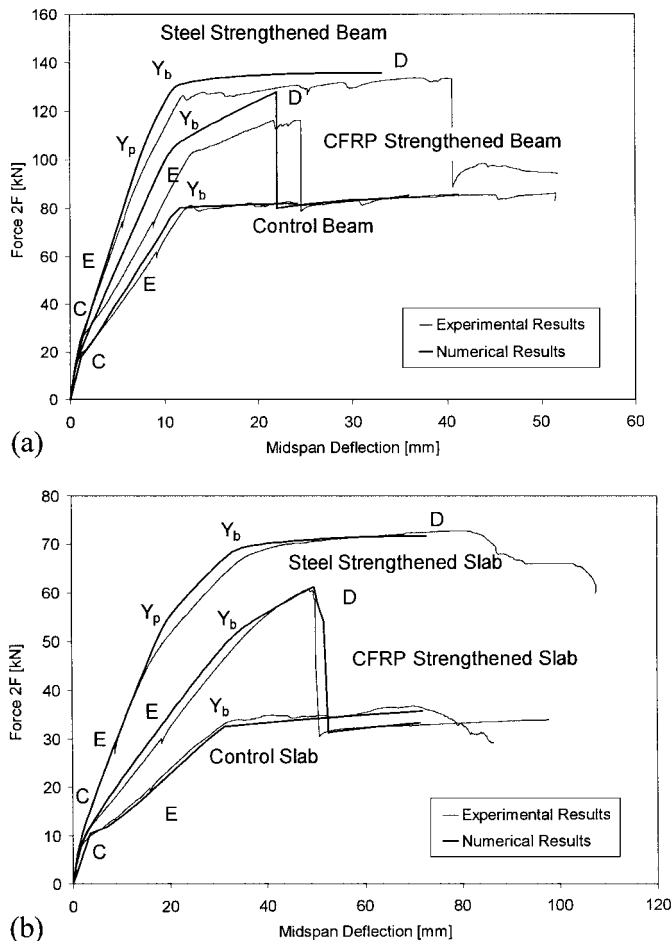


FIG. 5. Experimental and Numerical Results for: (a) Beams; (b) One-Way Slabs

and the slabs [Fig. 5(b)]. The proposed model yields a good estimate of both the stiffness and the strength of all the tested beams. A few meaningful points are labeled on the curves. Point *C* marks the onset of concrete cracking in the middle third of the beam and is followed by a drop in the beam stiffness. Point *E* represents a generic point during loading at which cracking spreads toward the beam support but the bottom steel rebars are still elastic. At point Y_b the bottom steel rebars yield, leading to a further drop in the response stiffness. For the case of the RC beams strengthened with the steel plate, Y_p indicates the point where the plate steel yields. As expected, the plate yields (point Y_p) before the longitudinal reinforcement yields (point Y_b). After the longitudinal reinforcement yields in the steel-strengthened and in the control beams, the response stiffness is very small and mainly due to the hardening properties of the reinforcement steel. On the contrary, for the beams strengthened with CFRP plate, after point Y_b the response stiffness is still considerable because of the elastic contribution of the strengthening plate. At point *D* plate debonding occurs. One can observe from the figures that, except for the slab strengthened with the steel plate, after point *D* both the experimental and the numerical responses show a large drop in beam strength because of the loss of the plate contributions. The residual strength is that of the original, non-strengthened RC beams.

The tension force distributions in the strengthening plate along the beam for the case of the RC beam of Fig. 4(a) are shown in Fig. 6. The different curves refer to the load levels labeled *E*, Y_b , Y_p , and *D* in Fig. 5(a) for the beam. Similar trends were observed in the slab. Consider the case of the CFRP plate [Fig. 6(a)]. As expected, the force in the plate is

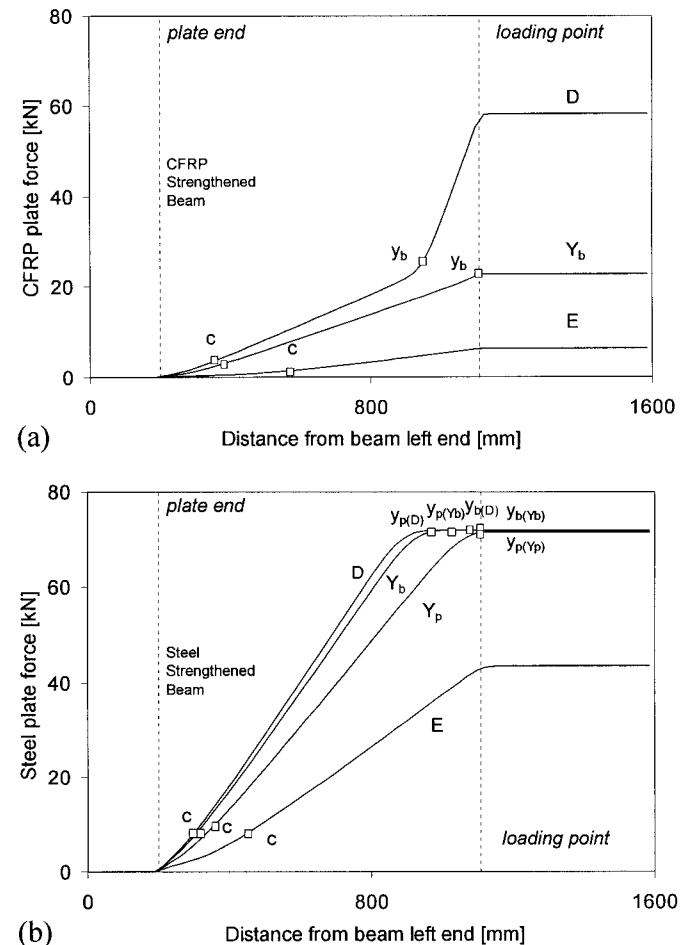


FIG. 6. Strengthening Plate Force Distributions for Beams with: (a) CFRP Plate; (b) Steel Plate

zero at the plate end (at 200 mm from the beam end), it increases up to the maximum value reached at the load application point (at 1,100 mm from the beam end), and it remains constant in the middle third of the beam, where the bending moment is constant. Two points on the force distribution mark a clear change in the force slope between the plate end and the load application point. The first point, labeled c in Fig. 6(a), separates the cracked (to the right of c) from the uncracked sections (to the left of c). Note that cracking never reaches the plate end section because failure by plate debonding happens first. The second point, labeled y_b in Fig. 6(a), corresponds to the section where the bottom steel rebars yield. The rebars are yielded to the right of point y_b and are still elastic to the left of it. Point y_b moves to the left from the distribution labeled Y_b to the distribution labeled D , indicating yield penetration as the load increases. If we now consider the case of the force distribution in the steel strengthening plate [Fig. 6(b)], note that the force in the steel plate cannot increase after yielding and the force maximum value is reached at load level Y_p whereas the force in the CFRP plate keeps on increasing until debonding occurs at load level D [Figure 6(a)]. Point y_p in Fig. 6(b) separates the region where the steel plate has already yielded (to the right of y_p) from the region where the plate steel is yet to yield (to the left of y_p).

The bond force distributions in the beam with CFRP plate, beam with steel plate, and slab with steel plate are shown in Figs. 7(a–c), respectively. The case of the slab with CFRP plate is similar to that of the beam with CFRP plate and is thus omitted. It is worth recalling that the bond force is proportional to the derivative of the force in the plate. Consequently, the bond stress is zero in the center third of the beam, where the shear force is zero.

From Fig. 7, it is observed that the bond force distribution for the steel and the FRP plates are quite different. For the CFRP strengthened beam [Fig. 7(a)], starting from the point where the load is applied and moving to the left toward the beam support, the bond force distribution gradually decreases except for two main points of discontinuity: one at the plate end and the other near the loading point. The bond discontinuity at the free end, due to the sudden change in cross section, is a well-known phenomenon; among the many studies available in the literature, see Roberts (1989), Täljsten (1997), Malek et al. (1998), and Rabinovitch and Frostig (2000). The bond discontinuity at the load application point is due to the sudden drop in the plate tensile force outside the region of constant moment. This bond discontinuity becomes sharper as larger loads are applied, but the largest increases are due to the rebar yield penetration along the beam. More specifically, for the bond force distribution corresponding to load level E , bond increases sharply near the point of load application and then decreases up to point c , which separates cracked and uncracked regions. The bond force drops to almost zero at point c . At loading level Y_b , the bond distribution drops drastically after the peak point (near the load application point) and remains constant over the cracked region where the steel rebars are still elastic. A similar bond force distribution is observed at load level D , but the bond force values are larger and there is a short plateau of almost constant bond after the peak. This plateau, which corresponds to the region where the bottom steel has yielded, ends roughly at point y_b , beyond which the bottom steel is still elastic. In Fig. 7(a), the bond force peak at load level D equals the epoxy resin strength very close to the load application point. This confirms the experimental observations by Zarnic et al. (1999), in which debonding initiated near the load application point.

The bond force distributions for the steel-strengthened beam are shown in Fig. 7(b). In this case, the bond force is zero near the load application point, up to the point y_p , which marks

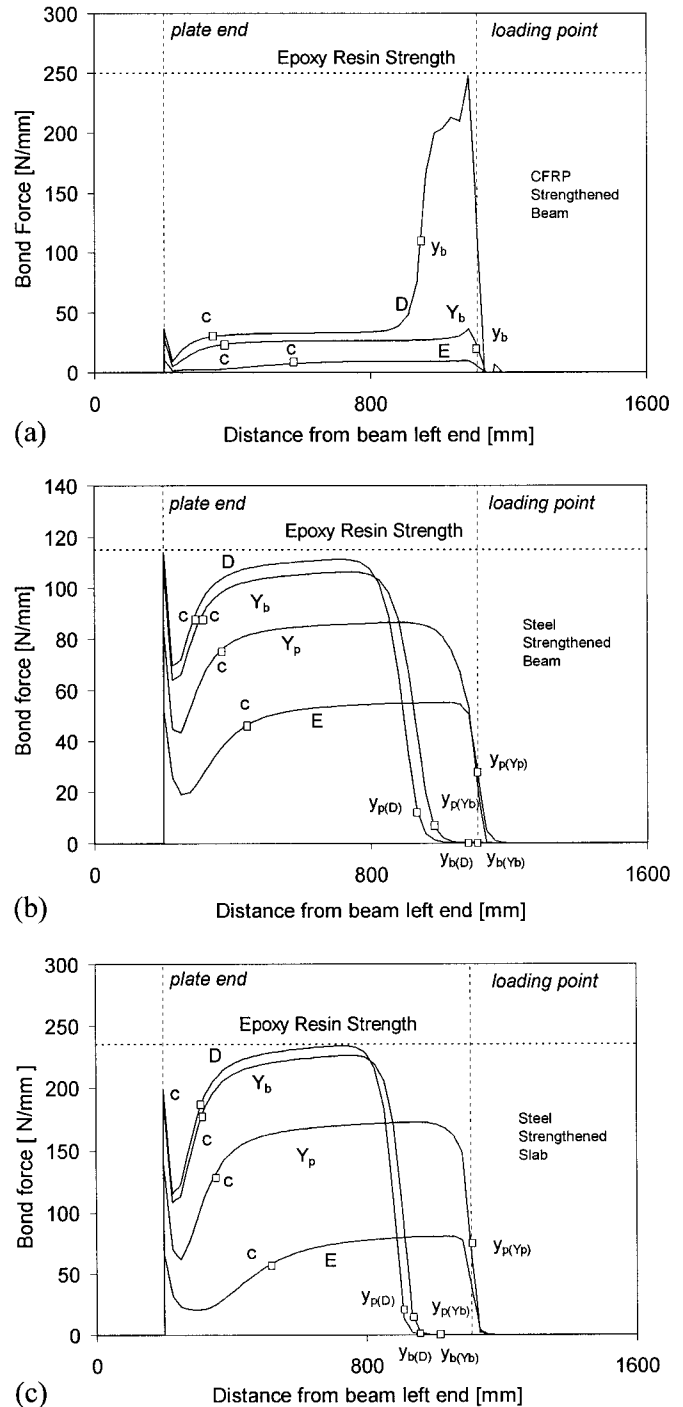


FIG. 7. Bond Force Distributions for: (a) Beam with CFRP Plate; (b) Beam with Steel Plate; (c) Slab with Steel Plate

the separation between yielded and nonyielded plate steel. Directly to the left of point y_p , the bond force sharply increases from zero to an almost constant value until point c , beyond which the concrete is uncracked. Finally, a sharp discontinuity arises at the plate end, which in this case represents the maximum bond value for the total length of the plate. As the load level increases, the plate steel yield front (point y_p) moves to the left and, consequently, the bond discontinuity and the intermediate plateau values increase too. This bond force increase is due to the shortening of the plate anchorage length, which spans from point y_p to the plate end. As steel yielding penetrates toward the plate end, the anchorage length decreases and the bond forces must increase to maintain equilibrium. According to Fig. 7(b), debonding starts at the plate end

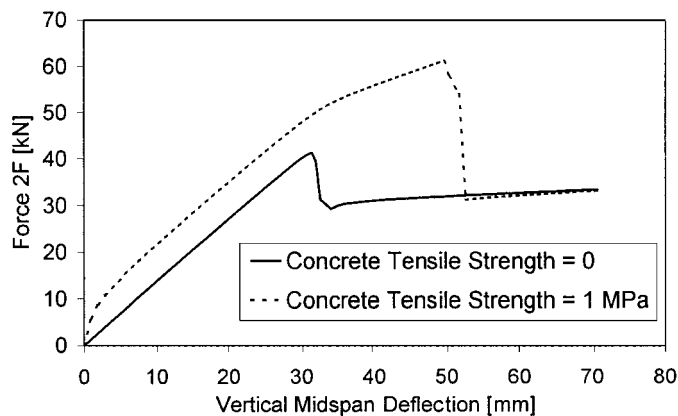


FIG. 8. Influence of Concrete Tensile Strength on Applied Load to Midspan Deflection for CFRP-Strengthened Slab

as soon as the bond force reaches the epoxy resin strength. These data confirm the experimental evidence reported by Zarnic et al. (1999).

Finally, Fig. 7(c) shows the bond force distributions for the case of the slab strengthened with the steel plate. The bond force distributions at different load levels are similar to those for the beam [Fig. 7(b)]. However, a main difference requires attention. At load level *D* the bond strength is reached between the plate end and the load application point. Furthermore, the bond strength is exceeded in a number of sections and not locally as in the cases of Figs. 7(a and b). This can probably explain why the failure mechanism of this beam was not clearly detected in the experimental investigation by Zarnic et al. (1999). The reinforced beam crushes immediately following debonding. This different failure mode can be justified by considering that the bond force peak that develops at the plate end (in the uncracked area) is more relevant as the beam stiffness increases (Roberts 1989; Oehlers and Moran 1990; Täljsten 1997). It follows that for the beam [Fig. 7(b)] this peak increases more rapidly than for the slab [Fig. 7(c)]. Finally, for the case of the CFRP strengthened slab, the bond force distributions are very similar to those derived for the CFRP reinforced beam [Fig. 7(a)]. These results are confirmed by the experimental observations available in the published literature (Arduini and Nanni 1997; Hörmann 1997).

Note that in this problem the model behavior is extremely sensitive to the tension stiffening behavior of the concrete (i.e., to the tensile strength f'_t) and to the postcracking behavior of the concrete after f'_t . It is shown in Fig. 8 that a very flexible solution is obtained when zero concrete tensile strength is considered. The reason is that this is a smeared crack model and the cracking effect is smeared along the element. Smeared crack models cannot represent local cracks in the region of constant moment and do not include the concrete contribution and the bond oscillations between cracks. The postpeak descending branch of the concrete in tension represents an average of the response of a beam region that includes cracked and uncracked sections between cracks. Finally, the choice of a relatively small value for f'_t was justified by the presence of early cracks (due to shrinkage and initial beam deflection) at the beam bottom before the plate was applied, as confirmed by the experimental report (Zarnic et al. 1999).

FAILURE MODES

From the experimental and numerical results plotted in Fig. 5, a few major observations can be drawn. First, thanks to the external strengthening, the loading capacity of the specimens is considerably increased. For the beams, average strength increases of around 53% with the steel plates and of 35% with the CFRP plates are obtained. For the slabs, the increase is

higher: very close to 98% with the steel plates and 73% with the CFRP plates. However, because of the debonding, this considerable strength increase is followed by the loss of the overall ductility for the reinforced beams and the slabs. Because the original, nonstrengthened beams are underreinforced, although the strength increases because of the external strengthening, the failure mode changes from ductile to brittle. All the specimens strengthened by means of steel plates show a ratio of failure-to-yield deflection that is sensibly larger than the same ratio for the specimens strengthened by means of CFRP sheets. Finally, a significant stiffness increase after cracking is measured: approximately 70 and 33% for the beams with steel and CFRP strengthening plates, respectively, and 145 and 72% for the slabs. The larger stiffness increase obtained with the steel plate rather than with the CFRP plate is mainly because the steel plate axial stiffness is more than twice the stiffness of the CFRP plate.

Both experimental results and numerical results clearly show that the ultimate failure condition for all the strengthened beams corresponds to debonding of the strengthening plate. Zarnic et al. (1999) observed that the CFRP plate detachment always initiates in the middle third of the beam, under the load application point, and propagates from there to the end of the plate by peeling off a very thin concrete layer (interface failure). For the case of the RC slabs strengthened with steel plates, detachment initiates at a point between the plate end and the load application point, with a typical interface failure. For the case of the RC beams strengthened with steel plates, plate detachment initiates at the plate end with the propagation of a horizontal splitting crack that causes spalling of the concrete cover under the longitudinal reinforcement. The overall tendencies of the experimental observations are confirmed by the numerical simulations presented in this work.

It is worth pointing out that, although debonding always initiates a sudden failure, debonding in the steel-strengthened beams happens long after the external plate has yielded and the maximum loading capacity has been reached, thus providing good ductility in the beam response (Fig. 5). On the other hand, in the CFRP-strengthened beams, the plate debonds when the beam response is still hardening, before the plate reaches its ultimate strength. In this latter case, the strengthening efficiency is not totally exploited because of an early detachment of the strengthening plate. In fact, the CFRP plate axial strains at debonding are 6.4 and 5.5‰ for the beam and the slab, respectively. These are approximately half the strains expected at the load level that would cause concrete crushing (assuming infinite bond strength).

With reference to the test results, it is possible to observe that the specimen failure is never due to concrete crushing or plate failure. Failure is always driven by a sudden loss of the composite action between the beam and the strengthening plate. Two distinct failure modes due to debonding can be identified:

- Mode A—Bond failure in an intermediate, cracked zone between the point of load application and the plate end
- Mode B—Bond failure at the plate end, where the concrete is still uncracked

The plate detachment from the concrete surface always happens when the bond stress value reaches the bond strength. However, Modes A and B are related to different failure mechanisms.

Mode A is linked to localized bond force peaks that typically happen around crack openings in tensile concrete areas. The smeared crack model used in this study cannot detect these peaks in a precise manner, and only a very detailed finite-element analysis would be able to capture such localized failures. The proposed model can however detect the zone

where the bond force peaks localize. The yield penetration from the point of load application toward the plate end is followed by a zone of bond force peak concentration where the steel has not yet yielded and the concrete has already cracked (Figs. 6 and 7). A further difference comes to light when one compares the elastic-brittle behavior of the CFRP strengthening plate with the elastoplastic response of the steel strengthening plate. In the first case, the plate force keeps increasing after the longitudinal rebar steel yields. Yielding of the rebars does not penetrate rapidly, because the strains are limited by the stiffness of the elastic CFRP plate. In this short zone next to the point of load application, the plate force sharply increases, thus causing a strong bond force localization around the load application point [Fig. 6(a) and Fig. 7(a)]. On the other hand, in the case of the steel strengthening plate, yielding of the external plate takes place first and propagates from the load application point along the beam pushing the bond force localization toward the plate end [Fig. 7(b)].

Mode B occurs when the bond force peak at the plate end (which typically falls in a zone of uncracked concrete) increases more rapidly than the internal localizations [Fig. 7(c)]. In this area, plate debonding induces a shear crack opening that develops within the concrete cover up to the rebar level, leading to a local splitting failure. The presence of even small peeling stresses acting on the spalled concrete cover probably influences this failure mode. However, it must be pointed out that the presented model can only identify the initial loss of bond between the concrete and the external plate and any interpretation of the failure mode itself is founded on the experimental evidence.

SUMMARY AND CONCLUSIONS

This paper studies the role of bond slip and of bond failure in RC shallow beams strengthened with either thin steel or thin CFRP plates. The study relies on a simple and accurate displacement-based fiber frame element with bond slip between the RC beam and the strengthening plate. Numerical simulations of a series of experimental tests by Zarnic et al. (1999) confirmed that the bond forces and the bond failure between the RC beam and the strengthening plates are fundamental issues in strengthening of shallow beams and must be taken into account to assess the effective stiffness and loading capacity of the strengthened member. In particular, implementation of an elastic-brittle bond-slip law yields detailed information on the evolution of the beam response under increasing applied loads. In particular, the following results were observed:

- Failure of the strengthened RC beams was always initiated by plate debonding.
- Beams strengthened by steel plates show a ductile response, mainly due to yielding of the strengthening plate, whereas beams strengthened by CFRP plates show a brittle response, because the response is dominated by the elastic behavior of the plate.
- Debonding starts somewhere between the point of load application and the plate end. In CFRP-strengthened beams, debonding tends to start under the point of load application, corresponding to a peak in the bond force distribution. In steel-strengthened beams, debonding starts either at the plate end or somewhere in the cracked concrete zone, depending on the beam depth.

The above observations confirm and complement the available experimental results and show the importance of using even simple numerical models to analyze the behavior of RC members. Future studies should concentrate on deep beams, where the interaction between shear stresses and bond slip may

cause different failure modes. Such a study necessitates the use of refined finite-element models that can capture the local evolution of the crack angles and the interaction of the cracks with the epoxy resin and with the slip in the longitudinal rebars.

ACKNOWLEDGMENTS

This study was supported by the University of Ferrara, Financial Founding EX60%-1998; Royal Thai Fellowship; and by Grant CMS-9804613 from the National Science Foundation, Washington, D.C. This support is gratefully acknowledged. The writers would also like to thank Prof. R. Zarnic of the University of Ljubljana, Slovenia, for providing the experimental data used in this paper. Many thanks also go to Prof. R. L. Taylor of the University of California, Berkeley, Calif., for his efforts to continuously enhance FEAP.

Any opinions expressed in this paper are those of the writers and do not reflect the views of the sponsoring agencies.

REFERENCES

- Arduini, M., Di Tommaso, A., and Nanni, A. (1997). "Brittle failure in FRP plate and sheet bonded beams." *ACI Struct. J.*, 94(4), 363–369.
- Arduini, M., and Nanni, A. (1997). "Behavior of precracked RC beams strengthened with carbon FRP sheets." *J. Compos. for Constr.*, ASCE, 1(2), 63–70.
- Bathe, K. J. (1996). *Finite element procedures*, Prentice-Hall, Upper Saddle River, N.J.
- Chajes, M. J., Finch, W. W., Jr., Januszka, T. F., and Thomson, T. A., Jr. (1996). "Bond and force transfer of composite material plates bonded to concrete." *ACI Struct. J.*, 93(2), 208–217.
- Holloway, L. C., and Leeming, M. B. (1999). *Strengthening of reinforced concrete structures*, CRC, London.
- Hörmann, M. (1997). "Post strengthening of concrete structures by externally bonded fiber reinforced polymers." *Diploma thesis, Inst. of Struct. Mech.*, University of Stuttgart, Stuttgart, Germany.
- Kent, D. C., and Park, R. (1971). "Flexural members with confined concrete." *J. Struct. Div.*, ASCE, 97, 1964–1990.
- Malek, A. M., Saadatmanesh, H., and Ehsani, M. R. (1998). "Prediction of failure load of RC beams strengthened with FRP plate due to stress concentration at the plate end." *ACI Struct. J.*, 95(1), 142–152.
- Menegotto, M., and Pinto, P. E. (1973). "Method of analysis for cyclically loaded reinforced concrete plane frames including changes in geometry and nonelastic behavior of elements under combined normal force and bending." *Proc., IABSE Symp. on Resistance and Ultimate Deformability of Struct. Acted on by Well-Defined Repeated Loads*, IABSE, Zurich, 112–123.
- Monti, G., and Spacone, E. (2000). "Reinforced concrete fiber beam element with bond-slip." *J. Struct. Engrg.*, ASCE, 126(6), 654–661.
- Oehlers, D. J., and Moran, J. P. (1990). "Premature failure of externally plated reinforced concrete beams." *J. Struct. Engrg.*, ASCE, 116(4), 978–995.
- Rabinovitch, O., and Frostig, Y. (2000). "Closed-form high-order analysis of RC beams strengthened with FRP strips." *J. Compos. for Constr.*, ASCE, 4(2), 65–74.
- Roberts, T. M. (1989). "Approximate analysis of shear and normal stress concentrations in the adhesive layer of plated RC beams." *The Struct. Engrg.*, 67(12), 229–233.
- Rubiano-Benavides, N. R. (1998). "Predictions in the inelastic seismic response of concrete structures including shear deformations and anchorage slip." *PhD dissertation*, Dept. of Civi. Engrg., University of Texas, Austin, Tex.
- Saadatmanesh, H., and Ehsani, M. R. (1991). "RC beams strengthened with GFRP plates. I: Experimental study." *J. Struct. Engrg.*, ASCE, 117(11), 3417–3433.
- Saadatmanesh, H., and Malek, A. M. (1998). "Design guidelines for flexural strengthening of RC beams with FRP plates." *J. Compos. for Constr.*, ASCE, 2(4), 158–164.
- Spacone, E., Filippou, F. C., and Taucer, F. F. (1996). "Fiber beam-column model for nonlinear analysis of R/C frames. Part I: Formulation." *Earthquake Engrg. and Struct. Dyn.*, 25, 711–725.
- Spacone, E., and Limkatanyu, S. (2000). "Response of reinforced concrete members including bond-slip effects." *ACI Struct. J.*, 97(6), 831–839.
- Täljsten, B. (1997). "Strengthening of beams by plate bonding." *J. Mat. in Civ. Engrg.*, ASCE, 9(4), 206–212.
- Taylor, R. L. (1999). *FEAP: A Finite Element Analysis Program User manual: Version 7.1*, Dept. of Civ. and Envir. Engrg., University of California, Berkeley, Calif., (<http://www.ce.berkeley.edu/~rlt/feap/>).

Zarnic, R., Gostic, S., Bosiljkov, V., and Bokan-Bosiljkov, V. (1999). "Improvement of bending load-bearing capacity by externally bonded plates." *Proc., Creating with Concrete*, R. K. Dhir and N. A. Henderson, eds., Thomas Telford, London, 433–442.

NOTATIONS

The following symbols are used in this paper:

$\mathbf{B}_u(x), \mathbf{B}_b(x)$ = beam and bond deformation-displacement matrices, respectively;
 $\mathbf{D}(x), \mathbf{d}(x)$ = section force and deformation arrays, respectively;
 \mathbf{K} = element stiffness matrix;
 $\mathbf{K}_B, \mathbf{K}_b$ = beam and bond contributions, respectively, to \mathbf{K} ;
 $\mathbf{k}_B(x), \mathbf{k}_b(x)$ = beam section and bond stiffness, respectively;
 $M_B(x)$ = beam section moment;
 $N_B(x), \bar{N}(x)$ = beam and plate axial forces, respectively;
 $\mathbf{N}_{uB}(x), \mathbf{N}_i(x)$ = beam and plate displacement shape functions, respectively;
 \mathbf{P} = element force array;
 $\mathbf{P}_B, \mathbf{P}_b$ = beam and bond contributions, respectively, to \mathbf{P} ;
 \mathbf{U} = element displacement array;
 $\mathbf{u}(x)$ = beam displacement arrays;

$\bar{u}(x), u_b(x)$ = plate axial displacement and relative slip, respectively;
 $u_B(x), v_B(x)$ = beam axial and transverse displacements, respectively;
 \bar{y} = plate distance from reference axis;
 $\epsilon_B(x), \bar{\epsilon}(x)$ = beam and plate axial strains, respectively;
 $\kappa_B(x)$ = beam curvature;
 ∂ = beam deformation differential operator

$$= \left\{ \begin{array}{cc|c} \frac{d}{dx} & 0 & 0 \\ 0 & \frac{d^2}{dx^2} & 0 \\ \hline 0 & 0 & \frac{d}{dx} \end{array} \right\}; \text{ and}$$

∂_b = bond deformation differential operator = $\{-1 \ \bar{y}(d/dx) \ 1\}$.